Cavitation Bubble Dynamics and Noise Production

Christopher E. Brennen
California Institute of Technology
Pasadena, California 91125, USA

Abstract

This paper presents a summary of some recent observations of the interaction between individual traveling cavitation bubbles and the nearly solid surface. These reveal a complex micro-fluid-mechanics associated with the interaction of the bubble with the boundary layer, the surface and the large pressure gradients exterior to the boundary layer which normally occur in the vicinity of a minimum pressure point. The details are important because they affect how the bubble collapses and therefore influence the noise produced and the damage potential of the cavitating flow. We present data showing how the noise from an individual event can be affected by these interaction effects. Since the scaling of cavitation phenomena is always an important issue we also describe the results of some experiments carried out to investigate the scaling of these interaction effects.

1. Introduction

The focus of this paper is on traveling bubble cavitation and the interactions between the flow and the bubbles which can occur in this type of cavitating flow. Traveling bubble cavitation occurs when small nuclei which are present in the liquid are convected into a region where the pressure is lower than the vapor pressure; the macroscopic vapor bubbles which are generated in this way then collapse when they are convected into regions of higher pressure. It is a well known property of potential flows that the point of minimum pressure must occur on the boundary of the flow. While boundary layer effects may modify this theorem and turbulent vortices may have low core pressures, it is nevertheless the case that cavitation frequently occurs close to a solid surface because this is where the minimum pressure is located. It follows that cavitation bubbles traveling through the low pressure region near the minimum pressure point will probably interact with that solid surface and may do so in a way which affects bubble collapse and the noise and damage potential of that collapse process.

In this paper we will review recent studies of the interactions between individual traveling bubbles and the flow in the vicinity of the minimum pressure region. We shall identify a number of important interaction phenomena and show that much of the detailed micro-fluid-mechanics associated with a single bubble (or "cavitation event") remains to be understood.

Before proceeding with these discussions it is important to emphasize that we will address only those circumstances in which the cavitation is limited so that the events

themselves do not interact. Thus we do not include bubble/bubble interactions which may become important when the concentration of bubbles becomes significant. We will also restrict discussion to traveling bubble cavitation but, in doing so, we also recognize that other types of cavitation can occur (vortex cavitation, attached or sheet cavitation) and will leave have own characteristic dynamics.

The dynamics of collapsing cavitation bubbles has received much attention since it was first recognized that the violence of the collapse was responsible for cavitation damage. In the early years Gilmore (1952) and Hickling and Plesset (1964) demonstrated how a collapsing and rebounding spherical bubble could produce a shock wave whose impingement on a nearby solid surface could, when repeated many times, cause local surface fatigue failure and consequently cavitation erosion. A second mechanism emerged from the work of Naude and Ellis (1961) (see also Benjamin and Ellis [1966]) who first observed that a collapsing spherical bubble collapsed in such a way that a high-speed, re-entrant "microjet" was formed which was directed at the nearby solid surface. Subsequent experimental and analytical observations (for example, Plesset and Chapman [1970], Lauterborn and Bolle [1975], Shima and Nakajima [1977], Shima *et.al.* [1981]) have provided a substantial literature on this phenomenon which is reviewed in Blake and Gibson (1987). However, the connection between the microjet and cavitation damage was not at all clear until recently. In a pair of important papers, Shima *et.al.* (1983) and Fujikawa and Akamatsu (1980) demonstrated by observations that the bubble collapse caused substantial impulsive pressures and stress waves within a nearly solid and, more recently, Kimoto (1987) showed that both the microjet and the subsequent collapse of the remnant bubble cloud can generate significant stresses in the solid.

From the perspective of this paper, it is, however, important to emphasize that almost all of this research has focused on bubble collapse in a *quiescent* liquid. Until the recent work of van der Meulen and van Renesse (1989), Ceccio and Brennen (1991), Kumar and Brennen (1991, 1992), and Kuhn de Chizelle *et.al* (1992), very little attention had been paid to the effect of the flow on the collapse process.

2. Headform Experiments in the Low Turbulence Water Tunnel

Ceccio and Brennen (1991) recently made a detailed examination of the dynamics and acoustics of individual cavitation bubbles occurring in the flow around two axisymmetric headforms. The experiments were carried out in the Low Turbulence Water Tunnel (LTWT) at the California Institute of Technology (Gates, 1977) and utilized a 5.08 cm diameter Schiebe headform (Schiebe [1972], Gates *et.al.* [1979], Meyer, Billet, and Holl [1989]) and a 5.59 cm ITTC headform (Lindgren and Johnsson [1966], Hoyt [1966]). The shapes and surface pressure distributions for these two headforms are shown in figure 1.

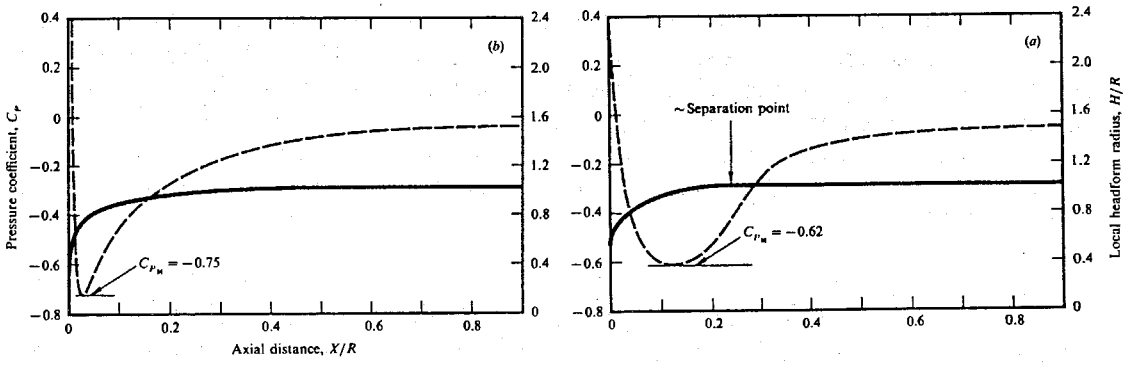

Figure 1. Shapes and surface pressure distributions for the Schiebe headform (left) and the ITTC headform (right) from Gates *et.al.* (1979) and Hoyt (1966), respectively. C_P is the pressure coefficient, X is the axial distance from the stagnation point, R is the final body radius and H is the local headform radius.

These headforms were equipped with two novel instrumentation systems. The first of these allowed the measurement of the noise produced by individual bubbles or "events." Most of the data on cavitation noise which appears in the literature was obtained using hydrophones on or outside of the walls of the water tunnel (for example, Barker [1975]). This has two difficulties. First the hydrophone is rather far from the source of the noise and second, the signal is often contaminated by acoustic reflections within the facility. To overcome this the present headforms were fabricated from lucite, a material whose acoustic impedance is a fairly good match to that of water. The hollow interiors of both bodies were then filled with water and the hydrophone was placed in this water on the axis of the body. Thus the headform and its interior is almost acoustically transparent and the signals from the cavitating bubbles can be recorded by a hydrophone which is close to the cavitation and without contamination by acoustic reflection. The hydrophone was an ITC-1042 model with a relatively flat response up to 80 kHz and the output was digitized at a sampling rate of 1 MHz. Confirmation of the effectiveness of this acoustic measuring system was obtained by comparing the output with that of a second hydrophone placed exterior to the headform (Ceccio, 1990).

The second, novel instrumentation system consisted of a series of electrodes on the surface of the headform which were used to detect and measure individual cavitation bubbles (Ceccio, 1990). This was adapted from an earlier impedance probe used to measure volume fractions in multiphase pipe flows (Bernier, 1981). The electrodes were made from an electrically conducting epoxy and were machined with the headform in order to prevent any roughness which might trigger or modify the

cavitation. A pattern of alternating electric potentials was applied to this electrode array and the current from each electrode was monitored. When a bubble passes over an electrode the impedance of the local conducting medium is altered causing a perturbation in the current from the electrode. This charge is measured and recorded and permits the position and volume of the bubble to be monitored during each cavitation event. Calibration is necessary for the measurement of bubble volume (see Ceccio, 1990).

Several different electrode geometries were utilized. Arrays of small, circular "patch" electrodes (seen in figure 2) were aligned in the flow direction and were used to follow the progress of cavitating bubbles on that particular streamline on the headform. They extended over most of the cavitating region. By using the output from these patch electrodes and an adjustable time delay to trigger an photographic flash unit, pictures could be taken of individual bubbles at prescribed locations on the headform surface. Thus the entire life cycle of a cavitation bubble could be explored. In addition to the "patch" electrodes, a series of "ring" electrodes which encircled the headform at a particular axial location were used to measure the total event rate.

The observations which follow were made at a series of different cavitation numbers, σ, defined as $2(p_\infty - p_v)/\rho U^2$ where p_∞, p_v are the tunnel pressure and vapor pressure, ρ is the water density, and U is the tunnel velocity. The air content was usually about 6--7 ppm and the tunnel was normally run at a velocity, U, of 9 m/sec.

3. Observations of the Dynamics of Individual Bubbles

Figures 2 and 4 present typical photographs of cavitation bubbles on the Schiebe and ITTC headforms, respectively. Individual bubbles are depicted in simultaneous profile (left) and plan (right) views using two cameras but a single flash unit. A series of photographs of *different* bubbles has been assembled to demonstrate the typical evolution of an individual cavitation bubble.

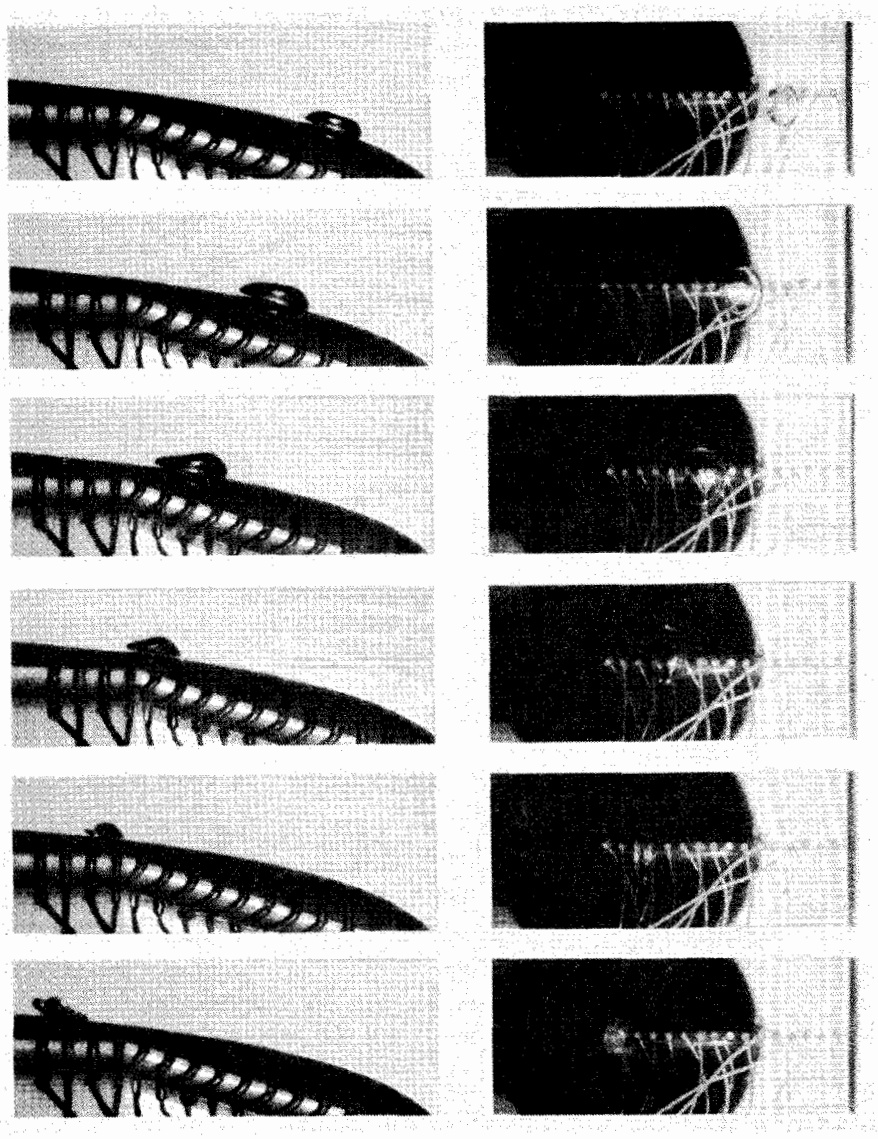

Figure 2. Series of photographs illustrating cavitation bubble evolution on the Schiebe headform. The conditions are $\sigma = 0.45$, $U = 9$ m/sec and the flow is from the right to the left.

Several important characteristics of cavitating bubble dynamics are illustrated in these photographs. In the initial phase of growth, the bubbles on both headforms behave similarly. Their shape is like that of a flattened hemisphere whose underside is separated from the headform surface by a thin film of liquid. From the earliest days of cavitation research, this hemispherical shape has been described (Knapp and Hollander [1948], Parkin [1952], Ellis [1952]) and remarks on this geometry occur fairly often in

the literature (for example, Blake *et.al.*, 1977). However, it is also the case that the circular shape apparent in the planform pictures has led some researchers to erroneously conclude that the bubbles are spherical.

The thickness of the thin film of liquid separating the bubble from the headform is of the same order of magnitude as the thickness of the laminar boundary layer and is therefore subjected to viscous shear stresses with important consequences which will be detailed later. It also follows that the outer surface of the bubble is acted on primarily by the irrotational flow outside the boundary layer. To help in understanding the bubble dynamics we include in figure 3 the typical isobars in the potential flow around the Schiebe body. Note that the pressure gradient normal to the surface in the vicinity of the low pressure region is larger than any pressure gradient experienced in the streamwise direction.

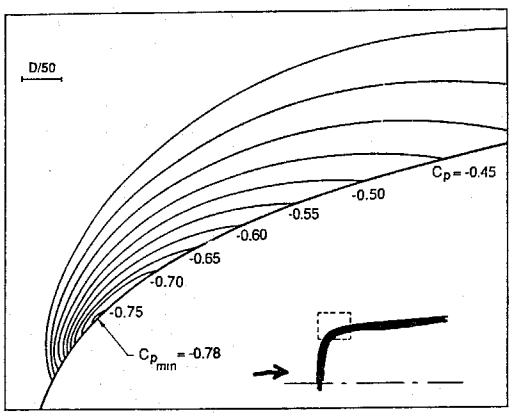

Figure 3. Isobars in the vicinity of the minimum pressure point on the Schiebe body from a potential flow solution of the flow. Values of the pressure coefficient, C_p, for each isobar are indicated.

The hemispherical shape of the growing bubbles is partly the result of the nearby solid surface interfering with the free growth of the bubble and partly the result of the bubble being forced toward the surface by the high pressure gradients normal to the solid surface. As the bubble reaches its maximum size it begins to experience higher pressures ahead and above it and so begins to deform into a wedge like shape shown in the third and fourth line of pictures in figure 2. At the same time its planform shape becomes distorted so that its dimension perpendicular to the streamlines is greater than its streamwise dimension.

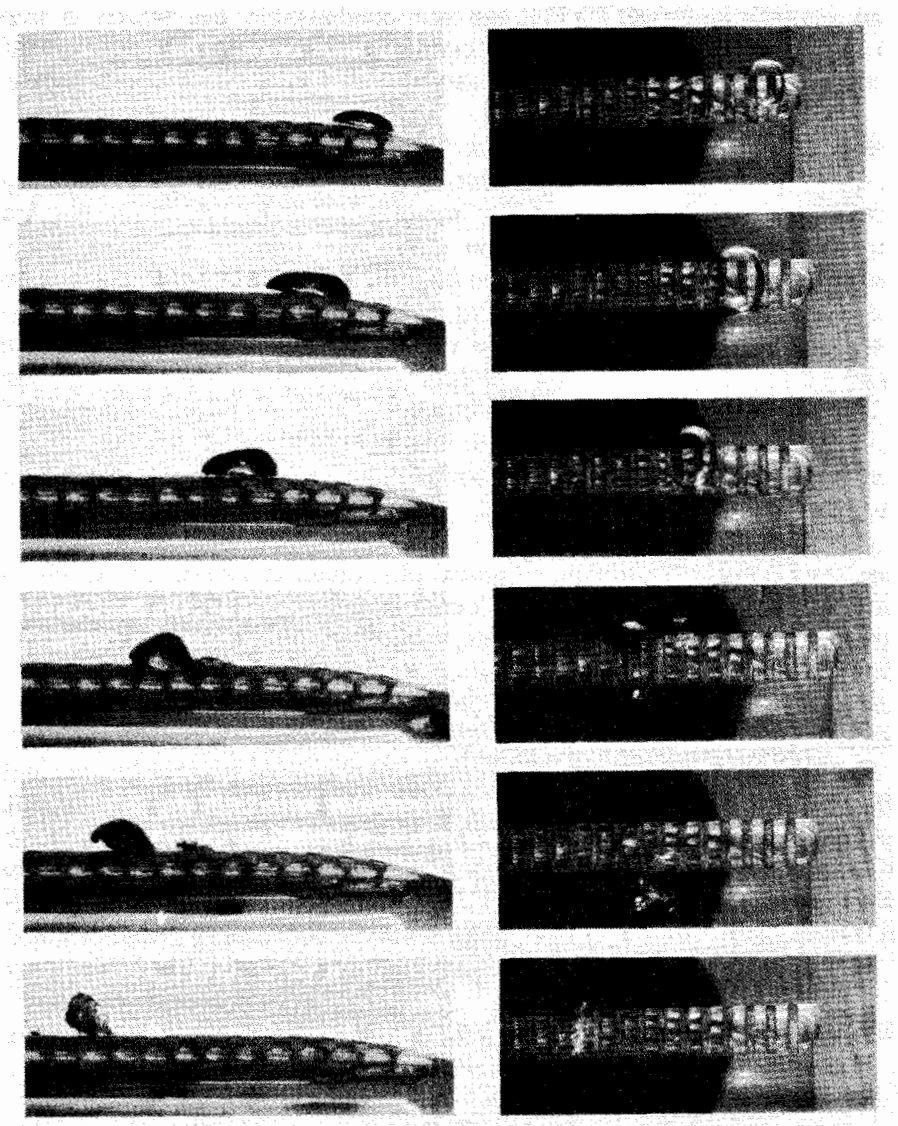

Figure 4. Series of photographs illustrating cavitation bubble evolution on the ITTC headform. The conditions are $\sigma = 0.45$ and $U = 8.7$ m/sec and the flow is from the right to the left.

The process of bubble collapse is a complex one and often the bubble will fission prior to collapse as seen in the fifth line of pictures in figure 2. Moreover, as it collapses, the circulation it has acquired becomes concentrated and the result is one or more small bubble/vortices as can also be seen in the fifth line. Thus the distortion of the planform shape takes the more extreme form of a bubble vortex of finite length. The fissioning of the bubble prior to collapse seems to lead to two separate collapses, each of which may

produce an acoustic pulse. Finally, the non-condensable gas which is inevitably present in the bubbles causes them to rebound at least once. The structures after the first rebound are clouds of smaller bubbles as illustrated by the last line of figure 2.

The Schiebe body was designed so that there was no laminar separation in the cavitation region (Schiebe, 1972). In contrast, the ITTC headform has a longer low pressure region and a laminar boundary layer separation (see figure 1). Because of these differences, the cavitation bubbles on the ITTC headform exhibited some differences in their dynamics as illustrated in figure 4. The bubble appears to ride up and over the separated region and, in doing so, the film underneath the bubble seems to become unstable. The roughening of the undersurface which results from this instability can be seen most clearly in the upper bubble in the right hand photograph of figure 5. The instability leads to the shearing off of a bubbly layer from the underside of the bubble as seen in the fourth and fifth lines of photographs in figure 4. This also implies a second and quite different mechanism of bubble fission but one which could also lead to more than one acoustic pulse.

Yet another important micro-fluid-mechanical phenomenon was observed with a small fraction of the bubbles on the ITTC headform and, occasionally, on the Schiebe body. This is illustrated in figure 5. In these cases, when the bubble passed a certain point on the headform surface (close to the separation point on the ITTC headform) it would trigger local attached cavitation at both lateral extremities. The upstream end of the tail is attached to the headform surface and the downstream end is connected to the bubble. Then, as the bubble moves on downstream, these attached streaks or "tails" are stretched out behind the bubble. Examples of bubbles with tails are shown in figure 5 and the right hand picture happened to catch two bubbles, one with tails and one without. While these events were quite rare in these experiments with 5 cm. diameter headforms we shall see that they feature much more prominently at higher Reynolds numbers.

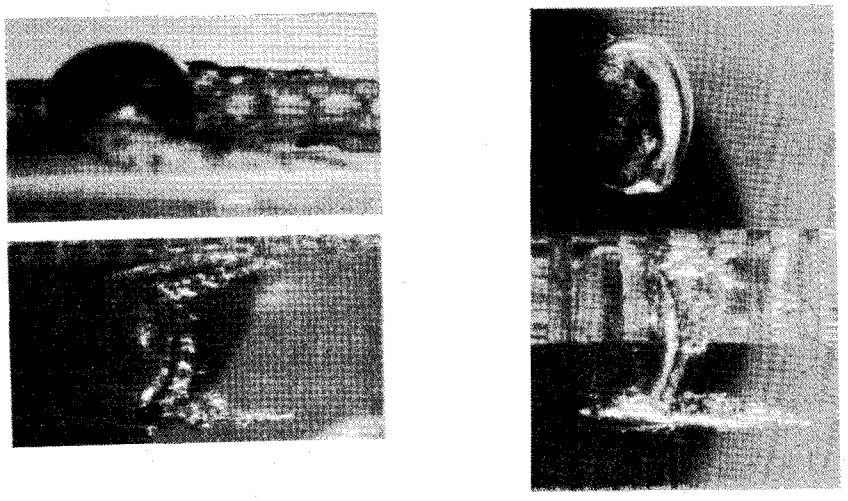

Figure 5. Examples of bubbles with tails on the ITTC headform at U = 9 m/sec and σ = 0.42.

4. Acoustic Emission of Single Cavitation Bubbles

Typical examples of the noise resulting from the first collapse as measured by the hydrophone are shown in figure 6 taken from Ceccio and Brennen (1991). Often a second acoustic pulse (or set of pulses) were recorded as a result of a second collapse which typically occurred about 600 μs after the first collapse. Statistics and data on the acoustic emissions are described in detail by Ceccio and Brennen (1991) and by Kumar and Brennen (1991, 1992). Only some highlights will be described here.

In the examples shown in figure 6, the first shows only one peak but the second is an example of the multiple peak events which occurred quite frequently. They are probably caused by bubble fission prior to collapse, though this is difficult to establish with certainty. We should also note that there was a great deal of uncertainty in the noise produced by individual bubbles so a large number of events had to be analyzed in order to detect any trends with speed and cavitation number. Sometimes an event would produce almost no detectable acoustic pulse. These mute events were not examples of "pseudo-cavitation," as observed by Dreyer (1987), but distinct cavitation events with a near-silent collapse.

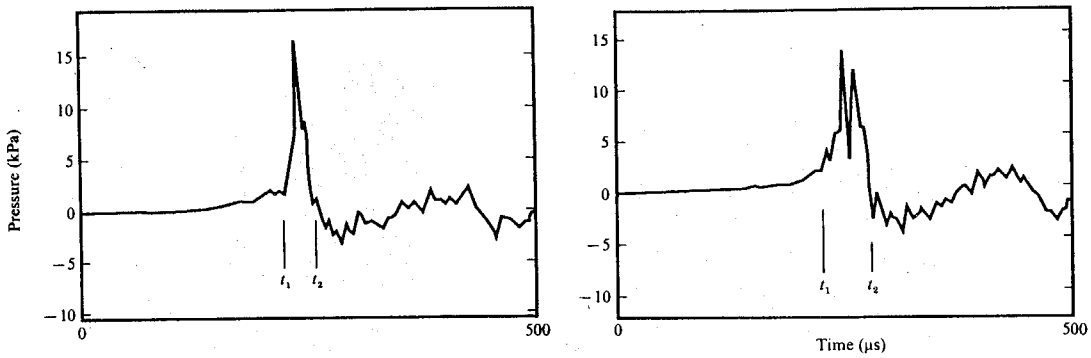

Figure 6. Two examples of the hydrophone output for individual cavitation bubble collapses (ITTC headform, U = m/sec, σ = 0.45) taken from Ceccio and Brennen (1991).

In these studies, the cavitation noise intensity is characterized by the acoustic impulse, I, defined as

$$I = \int_{t_1}^{t_2} p_A \, dt$$

where p_A is the hydroacoustic pressure pulse generated by the collapsing bubble and the times t_1 and t_2 were chosen to bracket the collapse pulse. Early in the investigation of the acoustic impulses it was recognized that the impulses were primarily correlated with the maximum size of the bubble as suggested by previous researchers (for example, Fitzpatrick and Strasberg [1956], Hamilton, Thompson and Billet [1982]). Therefore, we present the data on the impulses as a function of the maximum bubble size as measured by the electrode system (Ceccio, 1990). A typical array of data is shown in figure 7. Notice that all of the data appear to be below an envelope which seems to represent the maximum acoustic output which a collapsing bubble can generate if it collapses in some particular but unknown way. It can, however, produce less noise if it collapses in other ways.

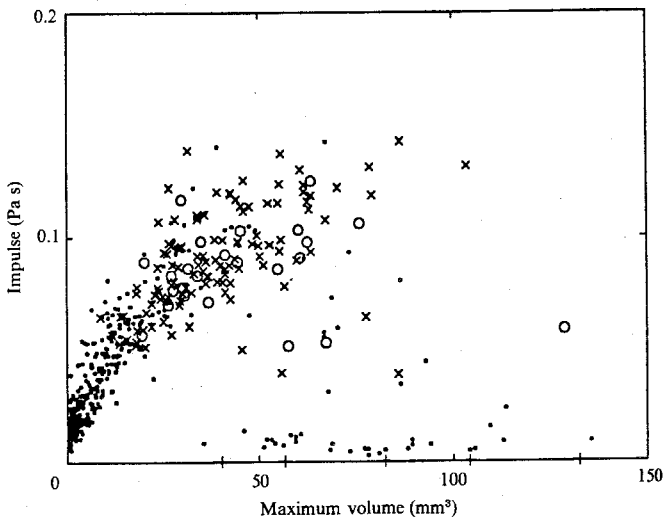

Figure 7. Acoustic impulse plotted against the maximum bubble volume for the Schiebe body at U = 9 m/s and σ = 0.42, + represents an event with no measured impulse, • an event with one acoustic peak, X an event with two peaks, O an event with more than two peaks.

In figure 7, different types of events are represented by different symbols. Notice that the probability of two or more peaks in the acoustic pulse increases with increasing size of the bubble, probably because larger bubbles are more likely to fission. Furthermore, it appears that the total impulse reaches a maximum when the bubble volume is about 40 mm^3. This maximum may also be caused by the fact that larger bubbles are likely to fission and that fissioning reduces the total impulse produced. But, also, it is likely that larger bubbles will contain more non-condensable gas as a result of dissolution and this would cushion the collapse and reduce the acoustic emission.

Though the bubble shapes are far from spherical, it is nevertheless of interest to compare the measured impulses with those which result from integration of the Rayleigh-Plesset equation for spherical bubbles. Though we could not expect quantitative agreement, such an analysis can provide a framework for exploring the parametric variations in single bubble noise and for anticipating the scaling laws which might apply to it. With these objectives in mind a program was written to calculate the variation in the radius or volume of a bubble as it traversed a given streamline close to the headform surface. Pressure distributions on such a streamline were constructed from knowledge of the surface pressure distribution (figure 1). The parameters included the initial nuclei radius far upstream (which determines the non-condensable gas content since the nucleus is assumed to be in equilibrium), the small offset from the stagnation streamline, a Weber number, a Reynolds Number and the cavitation number. Details are given elsewhere (Ceccio, 1990) and will not be repeated here. It is sufficient to point out that one can thereby obtain the volume $V(t)$, of the bubble as a

function of time, t, as it is convected around the headform and that one can then obtain the acoustic pressure, $p_A(r,t)$, as

$$p_A(r,t) = \frac{\rho}{4\pi r} \frac{d^2V}{dt^2}$$

Acoustic impulses could then be obtained for the collapse where t_1 and t_2 are the points at which $d^2V/dt^2 = 0$ on either side of the main collapse peak.

The calculations also show that the impulse correlates well with the maximum bubble volume almost independently of the parameters such as the cavitation number. Indeed, as indicated in figure 8 the curves are very similar for the two headforms. This figure also shows that the experimentally measured impulses are substantially less than those predicted by the Rayleigh-Plesset calculations. One can imagine that the spherically symmetric collapse is probably the most efficient noise producing geometry and that any departure from spherical symmetry leads to a less focused collapse and a smaller impulse. The data of both figures 7 and 8 suggest such a geometric effect on the acoustic efficiency. Moreover, the photographs of the bubbles on the ITTC headform show a more compact collapse than on the Schiebe headform and this, too, is consistent with the relative magnitudes of the experimental data in figure 8.

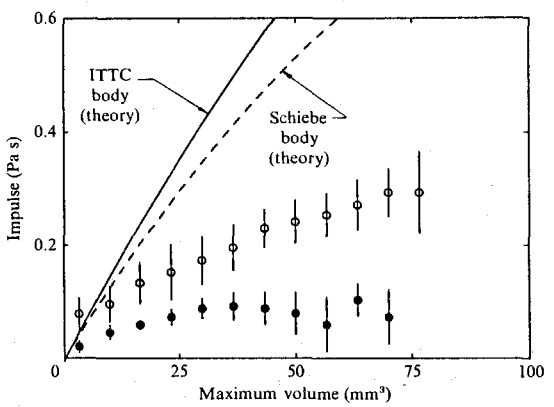

Figure 8. Comparison of theoretically predicted and experimentally measured acoustic impulse as a function of the maximum bubble volume for bubbles generated on the Schiebe body (open symbols) and ITTC body (closed symbols). Experimental data for $\sigma = 0.45$ and $U = 9$ m/s for the Schiebe body and $U = 8.7$ m/s for the ITTC body.

In their classic synthesis of cavitation noise, Fitzpatrick and Strasberg (1956) constructed spectra from the characteristics of the Rayleigh Plesset equation. While one should anticipate discrepancies due to the highly non-spherical nature of the actual bubble dynamics it is nevertheless of interest to Fourier analyze the present signals (such as in figure 6) to examine their frequency content. Typical results are shown in

figure 9 for three different ranges of cavitation number. These spectra are averaged over many different events in order to obtain characteristic results. Such averaged spectra will be equivalent to the spectra obtained from a long record containing many events provided the cavitation events occur randomly (Morozov, 1969). Note that the overall shape of the spectra vary little with cavitation number.

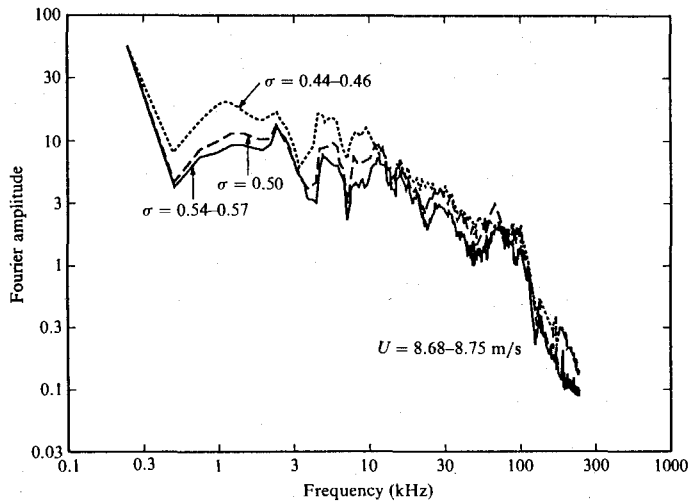

Figure 9. Averaged acoustic spectra derived from acoustic pulses generated by bubbles on the Schiebe body at average U = 8.7 m/s and σ = 0.45, 0.50, and 0.56. The vertical scale is arbitrary.

The slopes of the spectra in figure 9 are approximately -12 db/decade until about 100 kHz where the sharp fall off corresponds to the frequency response limit of the hydrophone. Thus the frequency dependence in the significant 10 → 100 kHz range is $f^{3/5}$ which is similar but not identical to the $f^{2/5}$ behavior obtained from a Rayleigh Plesset analysis (Blake, 1986). On the other hand, the experiments of Hamilton (1981) resulted in almost flat, frequency-independent spectra.

In closing, it may be appropriate to add a few remarks on the synthesis and prediction of cavitation noise. It is clear that this requires two fundamental inputs, namely a knowledge of the noise produced by individual events and a knowledge of the event rate. The first element, namely the character of individual events, has been explored analytically by Baiter (1974, 1986) and, in previous experiments, by Harrison (1952), Hamilton *et.al.* (1982), and Marboe *et.al.* (1986). With the present study there now exists a body of information on the first input. Provided there are not bubble/bubble interactions and provided the distribution of the events is random, we can expect to be able to synthesize the shape of the spectra from this input alone. Thus one would hope to understand, for example, the cavitation noise spectra of Blake *et.al.* (1977). When the

cavitation becomes more extensive so that bubbles interact, Arakeri and Shangumanthan (1985) have shown that the shape of the spectra change indicating a fundamental but as yet unknown change in the typical bubble dynamics.

The prediction of the magnitude of cavitation noise is much less well understood for it requires a method of predicting the event rate and therefore a model which connects the event rate with the free stream cavitation nuclei population. Since the nuclei population in any facility is likely to change with tunnel velocity, tunnel pressure and water quality, it follows that any experiments on or understanding of the scaling laws for cavitation noise requires knowledge of how the nuclei population changes with the operating condition. Apart from the important experiments of Keller (1972, 1974), little work has been done to understand the nuclei population dynamics in water tunnels and without such an understanding it will not be possible to understand the scaling of cavitation noise.

5. Scaling Experiments in the Large Cavitation Channel

The experiments described above were all performed with 5 cm. diameter headforms at a speed of about 9 m/sec. Consequently the issue of how the observed phenomena might scale with size and speed is an important one. Fortunately, the author was able to participate in an opportunity to investigate these scaling effects through a series of experiments on headforms conducted in the new water tunnel called the Large Cavitation Channel (LCC) operated by the David Taylor Research Center in Memphis, Tennessee (Morgan, 1990). The results of these experiments are described in detail elsewhere (Kuhn de Chizelle *et.al.*, 1992) and only a brief synopsis will be included here.

The LCC has a working section with a 3.05 m $\times$ 3.05 m cross-section; in the present experiments it was operated at three different speeds of 9, 11.5, and 15 m/sec. and two different dissolved oxygen contents of 30%, 80%, and 100% (though only results for 30% will be included here). The size of the facility allowed installation of identical Schiebe headforms measuring 5.08 cm, 25.4 cm, and 50.8 cm in diameter (figure 10). Consequently the range of Reynolds numbers which could be covered was between 5.4×10^5 and 9.4×10^6 or up to 17 times the Reynolds number of the earlier LTWT experiments.

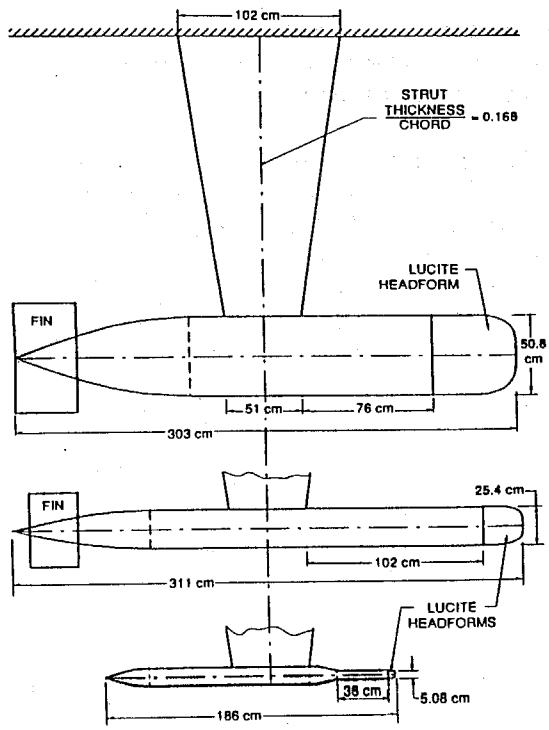

Figure 10. Schematic of the three Schiebe headforms installed in the Large Cavitation Channel.

All three headforms were made of lucite and were instrumented with an internal hydrophone and surface electrodes similar to the earlier experiments. In addition, two STI hydrophones with a flat response out to 100 kHz were installed in water filled recesses in the walls of the working section. Performing reciprocity tests with the STI and ITC hydrophones (using each in turn as a transmitter) the transfer gain spectra between each pair could be established under non-cavitating conditions. Using the manufacturer's response curves and the theoretical transfer function for the water, it was found that the mean error over the whole range of frequencies was less than 3 dB for all three headforms.

6. Cavitation Inception Data

Cavitation inception data was obtained on all the headforms by arbitrarily specifying a critical event rate of about one event every 5 seconds as detected by a patch electrode. This data is presented in figure 11, which clearly exhibits scale effects with headform size, tunnel velocity, and air content. The values of σ_i increase in air content and headform size much as one would expect. However, the marked decrease of σ_i with

velocity is less readily understood. We speculate that it may be caused by the decrease in the nuclei population of the tunnel at the higher pressures required to maintain the same cavitation number at a higher velocity.

For later reference note that at the inception cavitation number for the smallest, 5.08 cm headform, the cavitation is already quite extensive on the larger headforms. Thus the range of cavitation numbers during which there are a few traveling cavitation bubbles are quite different on the three headforms.

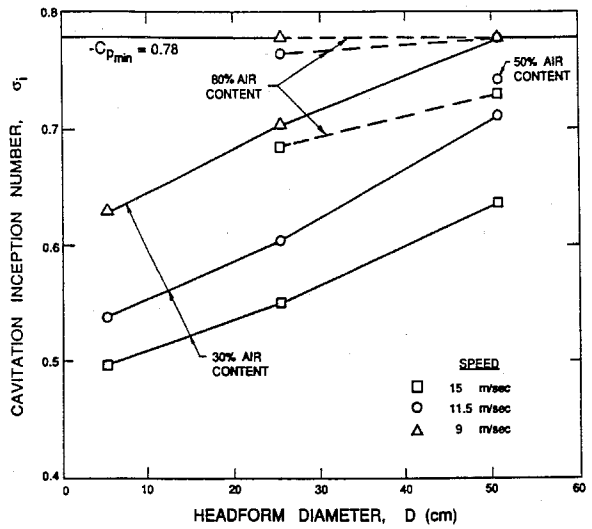

Figure 11. Cavitation inception numbers for the various headform sizes, tunnel velocities and air contents of the LCC experiments.

7. Observations on the Scaling of Bubble Dynamics

Most of the micro-fluid-dynamical phenomena described earlier were again observed during these tests so only the differences will be highlighted. The differences which were observed could be attributed to larger values of the Weber number or Reynolds number. The maximum value of the radius of the base of the hemispherical bubbles, R_{MAX}, is presented as a function of cavitation number in figure 12 and compares well with the spherical bubble radius calculated from the Rayleigh-Plesset equation.

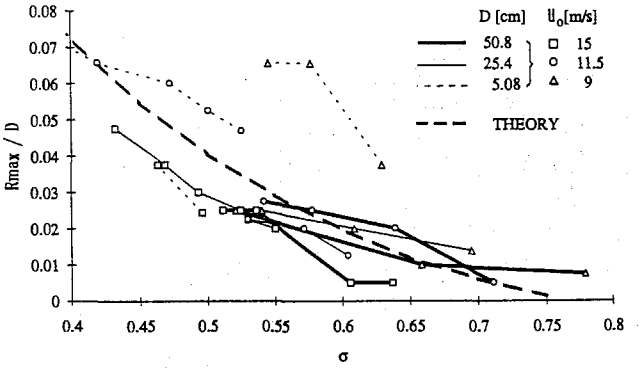

Figure 12. Maximum cavitation bubble dimension, R_{MAX}, defined as the radius of the base of the hemispherical cap plotted non-dimensionally against cavitation number for all headform sizes (D) and tunnel velocities. The radius of the spherical bubble calculated from the Rayleigh-Plesset equation is indicated by the heavy dashed line labeled theory.

Before describing the major changes in the bubble dynamics observed as the Reynolds number increased, there was one curious phenomenon which occurred and which seems to be the result of a decrease in the surface tension effects for the larger bubbles on the larger headform. Specifically, all of the bubbles appeared to have a very regular depression or "dimple" on their exterior surface as illustrated by the top picture in figure 13. This very regular feature was observed on all of the bubbles on the 25.4 cm and 50.8 cm diameter headforms and, in retrospect, lesser depressions could be detected in some of the earlier photographs of bubbles on the 5.08 cm headforms. It is not a re-entrant jet since it appears to be relatively static and persists through the growth and collapse phase (see Kuhn de Chizelle [1992] for other photographs of the dimple). It seems unlikely that this curiosity has significant consequences. One might speculate that it is the result of the large pressure gradient normal to the headform surface and that it is suppressed by surface tension effects in the smaller bubbles.

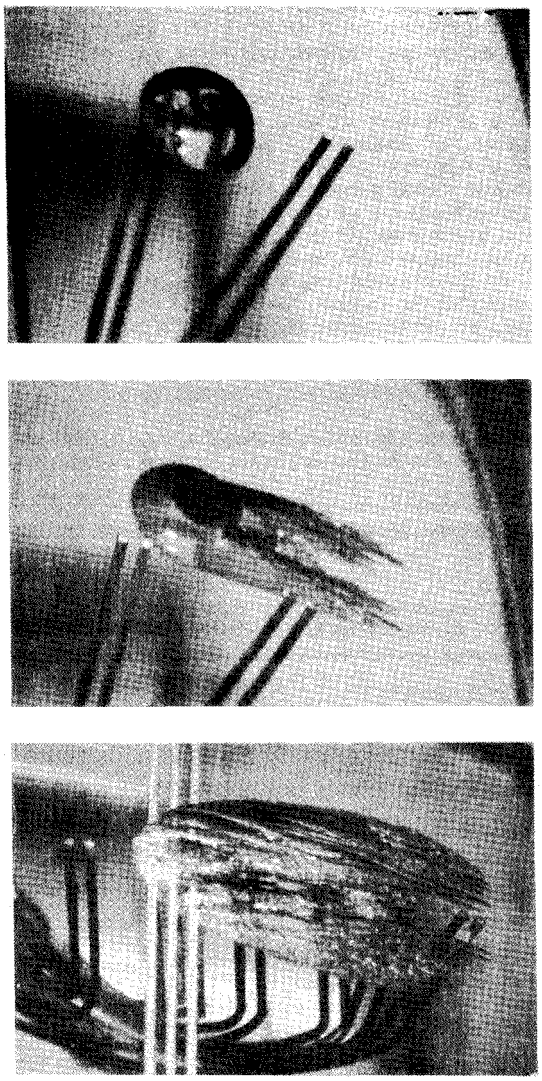

Figure 13. Photographs of typical events occurring on the 50.8 cm headform at U = 15 m/sec, and cavitation numbers in the range 0.55--0.60 and at 30% dissolved air content. For scale the distance between each of the pairs of patch electrodes is 2.54 cm.

In the earlier experiments on the small headform we observed that only occasional bubbles generated attached tails. In the present experiments we observed that the probability of a bubble generating attached tails increased both with speed and with headform size; it also increased with decreasing cavitation number. This increasing trend with higher Reynolds number is illustrated in the second photograph of figure 13. Whether or not a bubble will generate attached tails seems to be determined early in its life cycle. If no tails are generated, the smooth spherical cap of the top

photograph of figure 13 is the result. If tails are generated they always seem to attach at roughly the same streamwise location on the headform surface.

But other trends also emerged as the Reynolds number increased. The extent of the attached tails in the wake of the bubble seemed to increase as suggested by the second photograph in figure 13. Moreover, the tails seemed to persist for a brief time after the passage and collapse of the bubble. With further increase in Reynolds number this trend would evolve so that the bubble would trigger a large patch of attached cavitation as illustrated in the third photograph of figure 13. Moreover, this patch would often persist for some seconds after the triggering bubble had gone. At the highest Reynolds numbers it seemed as though the passage of traveling cavitation bubbles would trigger patches which would remain indefinitely. This may indeed be the universal mechanism for the formation of patch cavitation.

It is important to emphasize that, although we describe an evolution of cavitation events with increasing Reynolds number, there are no critical Reynolds numbers implied by this description. Rather, the probabilities of occurrence of each type of event change with increasing Reynolds number. Consequently, on the larger headforms one could observe bubbles without tails, bubbles with tails, and bubble-induced patches, all occurring at the same operating condition. The consequences of this evolution for cavitation noise will be discussed later.

8. Cavitation Noise Scaling

Data on the noise produced by individual events was processed in a manner similar to that used in the LTWT tests and is reported by Kuhn de Chizelle *et.al.* (1992). The typical acoustic impulses are presented using a non-dimensional impulse, I^*, defined by

$$I^* = 8\pi I / \rho UD$$

which is an appropriate non-dimensionalization according to the Rayleigh-Plesset analysis and should remove the scale effects of tunnel velocity and headform size. Data from all three headforms and at three tunnel speeds are presented in figure 14 as a function of cavitation number. The upper graph presents the average values of at least 40 of the larger events for each operating condition; the standard deviation is, however, large and is displayed in the lower graph.

Note first that the dimensionless acoustic impulse has the same order of magnitude for all of the data so it crudely adheres to the anticipated Rayleigh-Plesset scaling. Moreover, as the cavitation number is decreased, almost all of the data sets show an initial increase in the impulse, followed by a decrease at lower σ. The initial increase is clearly a consequence of the bubbles becoming larger at lower cavitation numbers. The subsequent decrease is caused by an increase in the number of bubbles with tails and

the fact that such bubbles produce less noise. We shall demonstrate this effect shortly. However, before leaving figure 14 we note that, if the data sets were shifted horizontally so that their cavitation inception numbers (figure 11) coincided, then the curves would correspond much more closely.

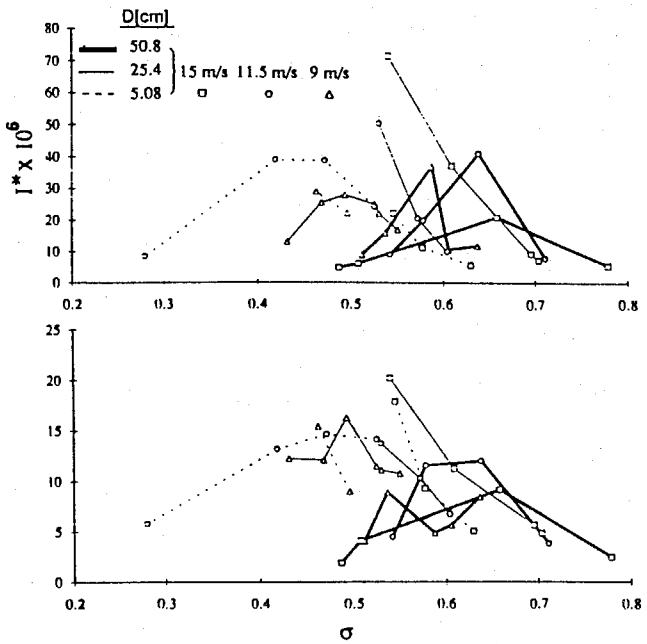

Figure 14. Top graph: average dimensionless impulse for 40 of the larger events at each operating condition. Lower graph: the corresponding standard deviations.

It was speculated that the decrease in the impulse at lower cavitation numbers was caused by an increasing fraction of the bubbles generating tails. This was proven in the following way. Events without tails could be distinguished from those with tails by the radically different electrode signals generated by the two kinds of events. As demonstrated in figure 15, the electrode signals from events without tails are brief as the bubble quickly passes over that electrode.

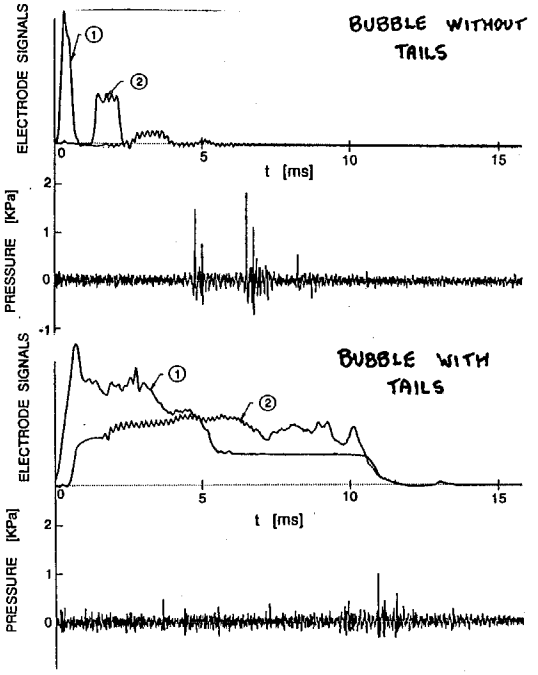

Figure 15. The typical electrode and hydrophone signals from an event without tails (upper traces) and an event with tails (lower traces). Signals from the first two electrodes are shown labeled (1) and (2).

On the other hand, the persistence of tails leads to a much longer duration of electrode signal perturbation. Consequently, as a diagnostic tool only, we may define a quantity γ_i (i = 1,2 are the first two electrodes) as

$$\gamma_i = \frac{U}{D}\int v_i(t)dt / (v_i)_{MAX}$$

where $v_i(t)$ is the electrode signal and the integration is performed over the entire perturbation to the electrode signal. Then, events with tails have much larger values of γ_i than those without tails. Moreover, in the latter category, the larger bubbles will tend to have somewhat larger values of γ_i.

To provide some averaging over the two electrode signals monitored during these tests, the value of $\gamma = \sqrt{\gamma_1 \gamma_2}$ was evaluated and a typical correlation of the dimensionless impulse, I^*, with this diagnostic parameter is shown in figure 16.

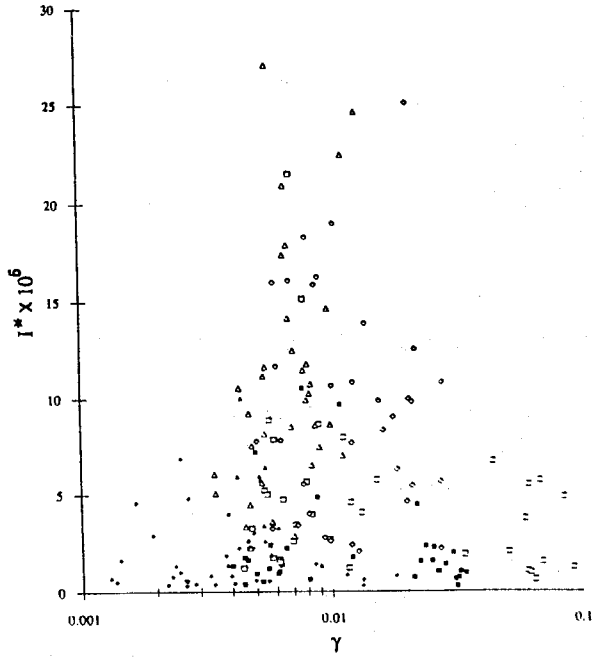

Figure 16. Correlation of the dimensionless impulse, I^*, with the diagnostic parameter, γ, for the 50.8 cm headform at 30% air content. Data is shown for U = 15 m/sec, σ = 0.64 (■); U = 15 m/sec, σ = 0.60 (□); U = 11.5 m/sec, σ = 0.71 (◆); U = 11.5 m/sec, σ = 0.64 (◊); U = 9 m/sec, σ = 0.78 (▲); U = 9 m/sec, σ = 0.66 (Δ).

Most of the data in this figure is for cavitation numbers close to inception in order to ensure no overlapping events.

This figure and others like it exhibit two characteristic upper limiting envelopes in the data. The data at low values of γ (0.001--0.005) exhibit an envelope of impulse which is increasing with increasing γ. This, of course, corresponds to an increase in the maximum impulse as the bubbles without tails get larger at lower cavitation numbers. But, in addition, there is an envelope on the right in which the maximum impulse decreases with increasing γ (γ = 0.02→0.1). We conclude that this shows that bubbles with tails yield significantly less noise than those without. This would, of course, be consistent with an earlier theme since the collapse of a bubble with tails is likely to be less focused than the collapse of one without tails.

Thus we conclude that the data on the noise from single events does, in general, exhibit the scaling expected based on the Rayleigh-Plesset equation. However, an important departure from this rule is that an increase in the Reynolds number increases the probability of an event producing tails or patches and that this significantly reduces the noise (and, perhaps, the damage potential) of that event.

9. Conclusions

This paper has provided a review of some research on the dynamics and acoustics of traveling cavitation bubbles. The research revealed complex micro-fluid-mechanics resulting from the interaction of the bubble with the headform surface and with the pressure gradients in the flow near the minimum pressure point.

Typical traveling cavitation bubbles have a spherical cap shape and are separated from the solid surface by a thin film of liquid which, in the present experiments, was comparable with the boundary layer thickness. In some conditions, this layer would become unstable, resulting in a sheet of small bubbles being left behind in the slower moving boundary layer fluid. But this was just one mechanism for bubble fission. The process of collapse of the bubbles is quite complex and results in small vortices of finite length whose axes are parallel with the solid surface and perpendicular to the flow. The vortices occur because of the circulation acquired by the bubbles in their interaction with the flow and the solid surface.

At lower Reynolds number, bubbles would occasionally trigger highly localized cavitation separation as they passed a certain location on the surface. The result is attached tails of cavitation which stretch out behind the bubble. As the Reynolds number is increased the probability of such events increases and the extent of the cavitation separation begins to spread laterally so that, eventually, the passage of a bubble triggers an attached patch of cavitation. Furthermore, with increased Reynolds number, the patches seem to persist longer, eventually remaining long after the bubble trigger has gone.

The typical linear dimensions of these traveling bubbles scales as the dimensions of a spherical bubble would scale according to the Rayleigh Plesset equation. The noise pulse produced by the collapse of each event also seems to scale roughly as the Rayleigh-Plesset analysis would predict. However, the magnitude of the acoustic impulse may be as much as an order of magnitude smaller than the theory would predict because the departure from sphericity disperses the focus of the collapse. Scale effects with Reynolds number do however occur because of the change in the triggering of attached cavitation or tails as the Reynolds number changes. Events with tails produce significantly less noise and, perhaps, are less damaging.

Acknowledgments

The author acknowledges the major contributions made to this research by students and former students at the California Institute of Technology and, in particular, Steven L. Ceccio (now at the University of Michigan), Sanjay Kumar (now at the Massachusetts Institute of Technology), and Yan Kuhn de Chizelle. I also appreciate the help given by

Douglas Hart (now at the Massachusetts Institute of Technology) and Zhenhuan Liu. The experiments in the D.T.R.C. Large Cavitation Channel would not have been possible without the help of W. M. Morgan, E. Rood, Young Shen, Scott Gowing, James Blanton, Bob Etter, and Po-wen Yu. The research was supported by ONR under contracts N00014-91-J-1295 and N00014-91-J-1426 and by the David Taylor Research Center. While I was preparing this manuscript in Kyoto, Japan, my teacher and friend, Arthur Arnold, passed away in a village halfway around the world. This paper is dedicated to him; I will miss him dearly.

References

Arakeri, V. H. and Shangumanthan, V. (1985). On the Evidence for the Effect of Bubble Interference on Cavitation Noise. *J. Fluid Mech.*, **159**, 131--150.

Baiter, H. J. (1974). Aspects of Cavitation Noise. *Symp. on High Powered Propulsion of Ships, Wageningen, The Netherlands*, **490**, 1--39.

Baiter, H. J. (1986). On Different Notions of Cavitation Noise and What They Imply. *Int. Symp. on Cavitation and Multiphase Flow Noise, ASME* **FED 45**, 107--118.

Barker, S. J. (1975). Measurement of Radiated Noise in the Caltech High Speed Water Tunnel -- Part II: Radiated Noise from Cavitating Hydrofoils. Guggenheim Aeronautics Lab., California Institute of Technology.

Benjamin, T. B. and Ellis, A. T. (1988). The Collapse of Cavitation Bubbles and the Pressures Thereby Produced Against Solid Boundaries. *Phil. Trans. Roy. Soc., London, Ser. A.*, **260**, 221--240.

Bernier, R. N. (1981). Unsteady Two-Phase Flow Instrumentation and Measurement. *Rep. E200.4*, California Institute of Technology.

Blake, J. R. and Gibson, D. C. (1987). Cavitation Bubbles Near Boundaries. *Ann. Rev. Fluid Mech.*, **19**, 99--124.

Blake, W. K., Wolpert, M. J. and Geib, F. E. (1977). Cavitation Noise and Inception as Influenced by Boundary-Layer Development on a Hydrofoil. *J. Fluid Mech.*, **80**, 617--640.

Blake, W. K. (1986). Mechanics of Flow Induced Sound and Vibration. *Introduction to Bubble Dynamics and Cavitation, Vol. 1*, Chap. 6, pp. 370--425, Academic Press.

Briancon-Marjollet, L. and Franc, J. M. (1990). Transient Bubbles Interacting with an Attached Cavity and the Boundary Layer. *J. Fluid Mech.*, **218**, 355--376.

Ceccio, S. L. (1990). Observations of the Dynamics and Acoustics of Travelling Bubble Cavitation. *Rep. E249.11*, California Institute of Technology, Division of Engineering and Applied Science.

Dreyer, J. J. (1987). Freestream Microbubble Effects on Travelling Bubble Cavitation Inception on the Schiebe Headform. *ARL/PSU Tech. Mem.*, 87--205.

Fitzpatrick, H. M. and Strasberg, M. (1956). Hydrodynamic Sources of Sound. *First Symp. on Naval Hydrodynamics, Washington, DC*, pp. 97--172.

Fujikawa, S. and Akamatsu, T. (1980). Effects of the Non-equilibrium Condensation of Vapour on the Pressure Wave Produced by the Collapse of a Bubble in a Liquid. *J. Fluid Mech.*, **97**, 481--512.

Gates, E. M. (1977). The Influence of Freestream Turbulence, Freestream Nuclei Populations and Drag Reducing Polymer on Cavitation Inception on Two Axisymmetric Bodies. *Rep.* E182-2. California Institute of Technology, Division of Engineering and Applied Science.

Gilmore, F. R. (1952). The Collapse and Growth of a Spherical Bubble in a Viscous Compressible Liquid. California Institute of Technology Hydrodynamics Laboratory, Rep. No. 26-4.

Hamilton, M. F. (1981). Travelling Bubble Cavitation and Resulting Noise. *Tech. Mem.* TM 81-70. Applied Research Lab., Pennsylvania State University.

Hamilton, M. F., Thompson, D. E. and Billet, M. L. (1982). An Experimental Study of Travelling Bubble Cavitation and Noise. *ASME Intl. Symp. on Cavitation Noise*, 25--33.

Harrison, M. (1952). An Experimental Study of Single Bubble Cavitation Noise. *J. Acoust. Soc. Am.*, **28**, 776--782.

Hickling, R. and Plesset, M. S. (1964). Collapse and Rebound of a Spherical Bubble in Water. *Phys. Fluids*, **7**, 7--14.

Hoyt, J. W. (1966). Wall Effect on I.T.T.C. Standard Head Shape Pressure Distribution. *11th Intl. Towing Tank Conf.*

Keller, A. P. (1972). The Influence of the Cavitation Nucleus Spectrum on Cavitation Inception, Investigated with a Scattered Light Counting Method. *ASME J. Basic Eng.*, Dec. 1972, 917--925.

Keller, A. P. (1974). Investigations Concerning Scale Effects of the Inception of Cavitation. *Proc. Conf. on Cavitation, Inst. Mech. Eng.*, 109--117.

Kimoto, H. (1987). An Experimental Evaluation of the Effects of a Water Microjet and a Shock Wave by a Local Pressure Sensor. *Int. ASME Symp. on Cavitation Res. Facilities and Techniques*, **FED 57**, 217--224.

Kuhn de Chizelle, Y., Ceccio, S. L., Brennen, C. E. and Shen, Y. (1992). Cavitation Scaling Experiments with Headforms: Bubble Dynamics. *Proc. Second Intl. Symp. on Propeller and Cavitation*, Hangzhou, China.

Kumar, S. and Brennen, C. E. (1991). Statistics of Noise Generated by Traveling Bubble Cavitation. *ASME Cavitation and Multiphase Flow Forum*, Portland, OR, June 1991, **FED 109**, 55--62.

Kumar, S. and Brennen, C. E. (1992). An Acoustical Study of Travelling Bubble Cavitation. Submitted to *J. of Fluid Mech.*

Lauterborn, W. and Bolle, H. (1975). Experimental Investigations of Cavitation Bubble Collapse in the Neighborhood of a Solid Boundary. *J. Fluid Mech.*, **72**, 391--399.

Lindgren, H. and Johnsson, C. A. (1966). Cavitation Inception on Headforms, I.T.T.C. Comparative Experiments. *Proc. 11th Intl. Towing Tank Conf, Tokyo.*

Marboe, M. L., Billet, M. L. and Thompson, D. E. (1980). Some Aspects of Travelling Bubble Cavitation and Noise. *Intl. Symp. on Cavitation and Multiphase Flow Noise, ASME* **FED 45**, 119--126.

Meulen, J. H. J. van der and Renesse, R. L. van (1989). The Collapse of Bubbles in a Flow Near a Boundary. *17th Symp. on Naval Hydrodynamics, The Hague*, 195--217. National Academy Press.

Meyer, R. S., Billet, M. L. and Holl, J. W. (1989) Free Stream Nuclei and Cavitation. *Intl. Symp. on Cavitation Inception, ASME* **FED 80**, 55--62.

Morgan, W. B. (1990). David Taylor Research Center's Large Cavitation Channel. *Proc. Int. Towing Tank Conf.*, Madrid, Spain, 1--9.

Morozov, V. P. (1969). Cavitation Noise as a Train of Sound Pulses Generated at Random Times. *Sov. Phys. Acoust.*, **14**, 361--365.

Naude, C. F. and Ellis, A. T. (1961). On the Mechanism of Cavitation Damage by Non-Hemispherical Cavities in Contact with a Solid Boundary. *ASME J. Basic Eng.*, **83**, 648--656.

Plesset, M. S. and Chapman, R. B. (1971). Collapse of an Initially Spherical Vapor Cavity in the Neighborhood of a Solid Boundary. *J. Fluid Mech.*, **17**, 283--290.

Scheibe, P. R. (1972). Measurement of the Cavitation Susceptibility of Water Using Standard Bodies. *Rep.* 118, St. Anthony Falls Hydraulic Laboratory, University of Minnesota.

Shima, A. and Nakijima, K. (1977). The Collapse of a Non-Hemispherical Bubble Attached to a Solid Wall. *J. Fluid Mech.*, **80**, 369--381.

Shima, A., Takayama, K., Tomita, Y. and Miura, N. (1981). An Experimental Study of Effects of a Solid Wall on the Motion of Bubbles and Shock Waves in Bubble Collapse. *Acustica*, **48**, 293--301.

Shima, A., Takayama, K., Tomita, Y. and Ohsawa, N. (1983). Mechanism of Impact Pressure Generation from Spark-Generated Bubble Collapse Near a Wall. *AIAA J.*, **21**, 55--69.